

**Vibhudutta Awasthi, Seong-Hwan Yee, Paul Jerabek, Beth Goins and William T. Phillips**

*J Appl Physiol* 103:28-38, 2007. doi:10.1152/jappphysiol.00136.2006

**You might find this additional information useful...**

---

This article cites 65 articles, 14 of which you can access free at:

<http://jap.physiology.org/cgi/content/full/103/1/28#BIBL>

Medline items on this article's topics can be found at <http://highwire.stanford.edu/lists/artbytopic.dtl> on the following topics:

- Biophysics .. Metabolism
- Medicine .. Resuscitation
- Medicine .. Cholesterol
- Medicine .. Hemorrhagic Shock
- Medicine .. Shock
- Physiology .. Rats

Updated information and services including high-resolution figures, can be found at:

<http://jap.physiology.org/cgi/content/full/103/1/28>

Additional material and information about *Journal of Applied Physiology* can be found at:

<http://www.the-aps.org/publications/jappl>

---

This information is current as of February 10, 2010 .

# Cerebral oxygen delivery by liposome-encapsulated hemoglobin: a positron-emission tomographic evaluation in a rat model of hemorrhagic shock

Vibhudutta Awasthi,<sup>1</sup> Seong-Hwan Yee,<sup>2</sup> Paul Jerabek,<sup>2</sup> Beth Goins,<sup>1</sup> and William T. Phillips<sup>1</sup>

<sup>1</sup>Department of Radiology and <sup>2</sup>Research Imaging Center, University of Texas Health Science Center at San Antonio, San Antonio, Texas

Submitted 22 February 2006; accepted in final form 16 January 2007

**Awasthi V, Yee S-H, Jerabek P, Goins B, Phillips WT.** Cerebral oxygen delivery by liposome-encapsulated hemoglobin: a positron-emission tomographic evaluation in a rat model of hemorrhagic shock. *J Appl Physiol* 103: 28–38, 2007; doi:10.1152/jappphysiol.00136.2006.—Liposome-encapsulated Hb (LEH) is being developed as an artificially assembled, low-toxicity, and spatially isolated Hb-based oxygen carrier (HBOC). Standard methods of evaluating oxygen carriers are based on surrogate indicators of physiology in animal models of shock. Assessment of actual delivery of oxygen by HBOCs and resultant improvement in oxygen metabolism at the tissue level has been a technical challenge. In this work, we report our findings from <sup>15</sup>O-positron emission tomographic (<sup>15</sup>O-PET) evaluation of LEH in a rat model of 40% hypovolemic shock. In vitro studies showed that PEGylated LEH formulation containing ~7.5% Hb and consisting of neutral lipids (distearoylphosphatidylcholine:cholesterol:α-tocopherol, 51.4:46.4:2.2) efficiently picks up <sup>15</sup>O-labeled oxygen gas. The final preparation of LEH contained 5% human serum albumin to provide oncotic pressure. Cerebral PET images of anesthetized rats inhaling <sup>15</sup>O-labeled O<sub>2</sub> gas showed efficient oxygen-carrying and delivery capacity of LEH formulation. From the PET images, we determined cerebral metabolic rate of oxygen (CMR<sub>O<sub>2</sub></sub>) as a direct indicator of oxygen-carrying capacity of LEH as well as oxygen delivery and metabolism in rat brain. Compared with control fluids [saline and 5% human serum albumin (HSA)], LEH significantly improved CMR<sub>O<sub>2</sub></sub> to ~80% of baseline level. Saline and HSA resuscitation could not improve hypovolemia-induced decrease in CMR<sub>O<sub>2</sub></sub>. On the other hand, resuscitation of shed blood was the most efficient in restoring oxygen metabolism. The results suggest that <sup>15</sup>O-PET technology can be successfully employed to evaluate potential oxygen carriers and blood substitutes and that LEH resuscitation in hemorrhage enhances oxygen delivery to the cerebral tissue and improves oxygen metabolism in brain.

oxygen carriers; blood substitutes; cerebral metabolic rate of oxygen; oxygen-15

THE OVERALL THERAPEUTIC GOAL of resuscitation in hemorrhagic shock is to maintain perfusion and oxygen delivery to the tissues (15). The usual practice of infusing crystalloids or colloids corrects the salt imbalance and the circulatory volume deficit in hemorrhagic shock, but neither fluid increases oxygen-carrying capacity in circulation. These fluids augment tissue oxygen delivery only by increasing cardiac preload and maintaining perfusion pressure. The only fluids that can increase both oxygen-carrying capacity as well as cardiac preload are the Hb-based products and red blood cells (RBCs) (5). For several reasons, Hb-based substitutes of RBCs are gradually

emerging as oxygen therapeutics for use in accidental blood loss, major surgery, or organ transport (47, 61). Besides being free of blood-borne pathogens, these products have the advantages of being easily purified, stored for a relatively long period of time, and used regardless of the recipient's blood type. An approach to encapsulate Hb inside lipid vesicles has recently commanded particular attention because of its lower toxicity compared with the molecularly modified forms of free Hb. Termed liposome-encapsulated Hb (LEH), it is an oxygen carrier that mimics the membrane-enclosed cellular structure of RBCs with respect to the oxygen transport and its eventual metabolic disposition in the reticuloendothelial system (RES) (33, 36, 38). The compartmentalization of Hb within a lipid bilayer potentially minimizes the cardiovascular and hemodynamic effects associated with other modified forms of Hb (21, 29, 37, 42, 57). With advanced encapsulation technology, it is also possible to coencapsulate reductants, antioxidative enzyme system, and oxygen-affinity modifiers with Hb to artificially resurrect the RBC environment (30, 53).

An important issue in resuscitation with oxygen carriers is the relationship between the oxygen-carrying capacity in circulation and oxygen utilization in the perfused tissue bed. It has not been clearly established whether the enhanced oxygen-carrying capacity in blood is reflected in an improved oxygen delivery and consumption in a hypoxic organ. For instance, in pediatric septic shock patients, it has been observed that even after the increase in hematocrit and Hb level by blood transfusion, there was no increase in oxygen consumption (27). If shock is defined as a condition where metabolic oxygen demand exceeds oxygen delivery (35), then monitoring oxygen delivery and metabolism is of paramount significance. Whole body imaging appears to satisfy this requirement when coupled with conventional hemodynamic monitoring in hemorrhagic shock. In this study, we utilized state-of-the-art small animal positron emission tomography (PET) and a positron-emitting isotope of oxygen, oxygen-15 (<sup>15</sup>O), as a physiological tracer for determining cerebral oxygen metabolism. We evaluated the capacity of LEH to improve cerebral metabolic rate of oxygen (CMR<sub>O<sub>2</sub></sub>) in a 40% hypovolemic shock model of rat. We also compared the performance of LEH with saline, shed blood, and 5% human serum albumin (HAS) as control resuscitation fluids. The results reveal that <sup>15</sup>O-PET technology can be successfully employed to evaluate oxygen carriers and blood substitutes and that LEH resuscitation delivers oxygen to cerebral tissue and improves oxygen metabolism in brain.

Address for reprint requests and other correspondence: V. Awasthi, Dept. of Pharmaceutical Sciences, College of Pharmacy, Univ. of Oklahoma Health Science Center, 1110 N. Stonewall Ave., Oklahoma City, OK 73117 (e-mail: vawasthi@ouhsc.edu).

The costs of publication of this article were defrayed in part by the payment of page charges. The article must therefore be hereby marked "advertisement" in accordance with 18 U.S.C. Section 1734 solely to indicate this fact.

## METHODS

**Materials.** The phospholipids distearoylphosphatidylcholine (DSPC) and poly(ethylene glycol)<sub>5000</sub>-distearoylphosphatidylethanolamine (PEG<sub>5000</sub>-DSPE) were obtained from Avanti Polar Lipids (Pelham, AL). Cholesterol (Chol) was purchased from Calbiochem (La Jolla, CA), and  $\alpha$ -tocopherol was purchased from Aldrich (Waukegan, IL). Glutathione (GSH), octyl- $\beta$ -glucoside (OBG), and pyridoxal 5'-phosphate were from Sigma (St. Louis, MO). The <sup>15</sup>O-labeled tracers were produced in Scanditronix model MC17F Cyclotron using <sup>15</sup>N(p,n)<sup>15</sup>O nuclear reaction. The anesthetics, xylazine and ketamine, were from Phoenix Scientific (St. Joseph, MO) and Fort Dodge Animal Health (Fort Dodge, IA), respectively.

**Isolation of stroma-free Hb from outdated RBCs.** The isolation of Hb involved hypotonic lysis of RBCs followed by several tangential-flow filtration steps. Outdated RBC units for Hb isolation were kindly provided by the South Texas Blood and Tissue Center (San Antonio, TX). To prevent temperature-sensitive degradation of Hb during isolation, storage, and LEH manufacturing, RBCs were carbonylated with filtered carbon monoxide (CO). The procedure was performed inside a laminar flow hood using endotoxin-free material and water for injection (62). The lysed blood was sequentially filtered through 0.65- $\mu$ m, 0.1- $\mu$ m, and 500-kDa hollow fiber filters (Amersham Biosciences, Piscataway, NJ). The bulk stroma-free Hb (SFH) was concentrated through a 10-kDa hollow fiber filter and stored frozen at -70°C.

**Preparation of LEH.** Neutral LEH (DSPC:Chol: $\alpha$ -tocopherol, 51.4:46.4:2.2) with postinserted PEG-DSPE was prepared by the technique reported previously (3). Figure 1 illustrates a typical LEH manufacturing procedure. Hb was in the form of CO-Hb (38 g/dl, <0.25 endotoxin units/ml). The manufacturing process was a combination of microfluidization and ultrafiltration. For PEGylation, PEG<sub>5000</sub>-DSPE solution was added to a dilute suspension of LEH, such that the concentration of PEG<sub>5000</sub>-DSPE was below its critical micelle concentration (44). To convert carbonyl-Hb back to oxy-Hb, the PEGylated LEH was exposed to a bright visible light from a 500-W halogen lamp under saturating oxygen atmosphere at 4–8°C (38). The final LEH preparation was suspended in 5% HSA.

**Characterization of LEH (Table 1).** The phospholipid concentration of the LEH was determined by the method of Stewart (46). The oxygen affinity ( $P_{50}$ ) was measured in a Hemox-analyzer (TCS Scientific, New Hope, PA). Amount of encapsulated Hb was determined by monitoring absorbance of the OBG lysate of LEH at 540 nm (54). Methemoglobin content was measured in Hb as well as LEH

Table 1. *Properties of LEH*

LEH Property	Value
(DSPC:Chol: $\alpha$ -tocopherol)-PEG-DSPE	51.4:46.4:2.2
$P_{50}$ , mmHg	19.9
Hb, g/dl	7.5
Phospholipid, mg/ml	59
Osmolality, mosmol/kgH <sub>2</sub> O	320
Oncotic pressure, mmHg	20.2
Methemoglobin, %	<5
Endotoxin, EU/ml	<0.25
Size, nm	193.5

LEH, liposome-encapsulated Hb; 51.4:46.4:2.2 is the distearoylphosphatidylcholine (DSPC):cholesterol (Chol):  $\alpha$ -tocopherol ratio; PEG-DSPE, poly(ethylene glycol)-distearoylphosphatidylethanolamine;  $P_{50}$ , oxygen affinity; EU, endotoxin units.

(26). The particle size was determined by photon correlation spectroscopy using a Brookhaven particle size analyzer equipped with argon laser, BI-9000AT digital correlator, and BI-200SM goniometer (Holtville, NY). Each sample was sized for 2 min with detector at 90° angle, and the sample was housed in a 25°C bath. The data were analyzed by non-negatively constrained least squares (CONTIN) using dynamic light-scattering software (9KDLSW, beta version 1.24) supplied with the instrument.

**Other resuscitation fluids.** Commercially available 0.9% normal saline (NS) and 5% HSA were used as control fluids for the resuscitation of animals. The fluids were chosen for comparison on the basis of their current clinical utility and availability. Five percent HSA solution was prepared by diluting a 25% human serum HSA solution (Albutein, Grifols Biological) with 0.9% saline. Since our LEH formulation contains 5% HSA, use of this fluid as one the controls was appropriate. Finally, shed blood was used as another fluid for comparison.

**Animal studies.** The animal experiments were performed according to the NIH Animal Use and Care Guidelines and were approved by the Institutional Animal Care Committee of the University of Texas Health Science Center at San Antonio. In the first phase of the study, we tested the capacity of LEH to carry oxygen and the feasibility of applying <sup>15</sup>O-micro-PET technique for imaging cerebral oxygen delivery in normal rats. There was no surgical procedure performed in this group of rats ( $n > 3$ ). This study also formed the basis of standardizing various protocols for subsequent investigation of cere-

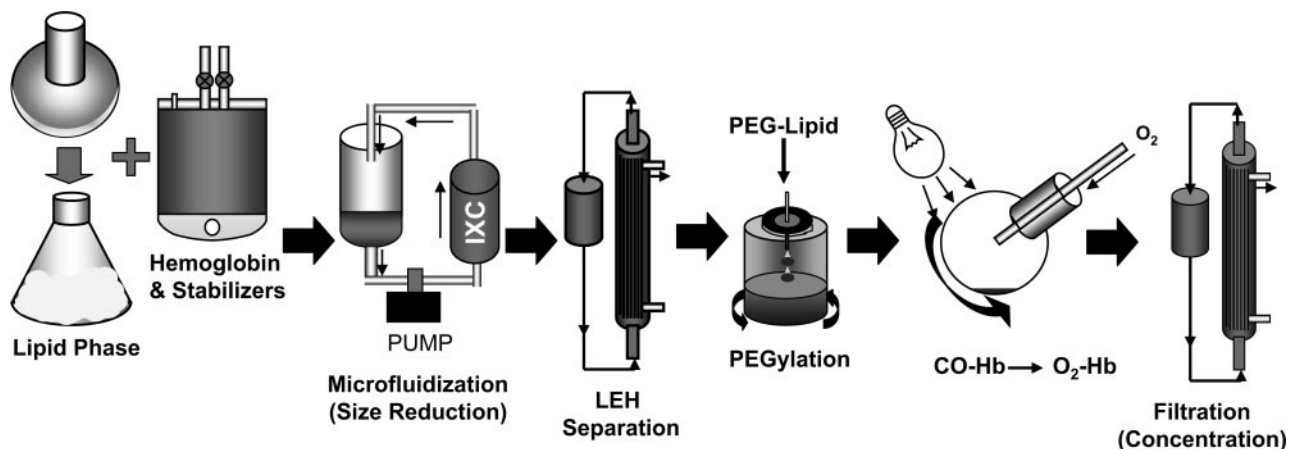


Fig. 1. Manufacturing scheme for liposome-encapsulated hemoglobin (LEH) preparation. Hydrated lipid phase is mixed with aqueous solution of CO-Hb, catalase, and other stabilizers. The mixture is microfluidized to reduce the particle size of LEH before filtering off unencapsulated CO-Hb (500-kDa molecular mass cutoff). The LEH preparation is taken for PEG-DSPE insertion at 55°C before converting CO-Hb to its oxy-form. In the final stage, dilute LEH is concentrated by ultrafiltration (500-kDa molecular mass cutoff). IXC, interaction chamber.

bral oxygen metabolism. A small sample of LEH was exposed to  $^{15}\text{O}$ -labeled  $\text{O}_2$  gas in a tonometer for 5 min. The rats were anesthetized by intramuscular ketamine-xylazine mixture (50 and 10 mg/kg body wt, respectively) and positioned inside a Rodent R4 Micro-PET detector (Concorde Microsystems, Knoxville, TN).  $^{15}\text{O}$ -labeled LEH (0.5 ml) was bolus injected intravenously through tail vein in a normal rat. As a comparison, a similarly processed  $^{15}\text{O}$ -labeled rat RBC preparation was also injected in an identical fashion. Rat RBCs were obtained from a donor rat. Imaging was performed for 4 min.

**Animal model of hemorrhagic shock and PET imaging.** The rat hypovolemic exchange transfusion model has been described earlier (14). Left femoral artery of male Sprague-Dawley rats (225–450 g) was cannulated with a polyethylene catheter. The catheter consisted of Tygon tubing (0.02 in.  $\times$  0.06 in.) coupled to a 2.5-in. polytetrafluoroethylene tip (28 gauge). The catheter was subcutaneously tunneled, secured at the nape, and filled with heparin (1,000 U/ml). After the surgical area was closed, the rats were given 2 days to recover from the procedure. On the day of the study, the rats were anesthetized by intramuscular ketamine-xylazine mixture (50 and 10 mg/kg body wt, respectively) and instrumented to digitally monitor rectal temperature and arterial blood pressure (iWorx, Dover, NH). For micro-PET imaging, the anesthetized animal was wrapped inside a warm water blanket and positioned inside the micro-PET detector. The imaging study was conducted according to the flow chart shown in Fig. 2. After the animal was allowed to stabilize,  $^{15}\text{O}$ -PET imaging was performed (baseline scan). The rat was insufflated with  $^{15}\text{O}$ -labeled  $\text{O}_2$  gas (5 ml, 1–2 mCi) using a specially designed nose cone. Image acquisition was performed for at least 4 min. Blood sample (0.2 ml) was withdrawn to determine hematocrit and to measure arterial oxygen content. At the end of the baseline study, 40% of circulating blood was withdrawn through the catheter at the rate of 0.5 ml/min. A constant-volume hemorrhage protocol was used because it has been suggested that it imitates clinical scenario more closely than the constant-pressure protocol (6). The volume of blood was estimated as 5.7% of the total body weight. The hypovolemic animal was allowed to stabilize for 30 min before a second  $^{15}\text{O}$ -PET scan and blood sampling was repeated (postbleed scan). Immediately after the post-bleed scan, the animal was isovolemically resuscitated at 0.5 ml/min with one of the resuscitation fluids. The animal was allowed to stabilize, and another set of  $^{15}\text{O}$ -PET imaging and blood sampling was performed (resuscitation scan). After imaging, the rat was euthanized by an overdose of euthanasia solution (Beuthesia, Veterinary Labs, Lenexa, KS).

Arterial oxygen content was estimated in the blood sample by a Co-Oximeter (1) (Avox Systems, TX). Since LEH interferes with the function of Co-oximeter, the Hb content in the LEH group was estimated on the basis of our previous report on circulation kinetics of LEH formulation in rats (4) and taking 95% Hb saturation as standard in the experimental conditions (Eq. 1). With a half-life ( $T_{1/2}$ ) of 30 h,  $\sim 99\%$  of injected LEH is in circulation at 30–60 min. We took into account the Hb content of LEH (7.5 g/dl) to calculate oxygen content of arterial blood in animals infused with LEH. No attempt was made to match Hb content of LEH to that of the shed blood:

$$\text{oxygen content (ml/dl)} = \frac{\text{Hb saturation} \times [\text{Hb}] \times 1.34 + 0.31}{100} \quad (1)$$

where 0.31 is the factor for oxygen dissolved in plasma at partial pressure of oxygen in air = 100 mmHg.

**Micro-PET image reconstruction.** The three-dimensional (3-D) PET data acquired in the list mode was rebinned into multiple frames of 1-s duration using a Fourier rebinning algorithm (11, 25). After rebinning the data, a 3-D image with a matrix size of  $128 \times 128 \times 63$

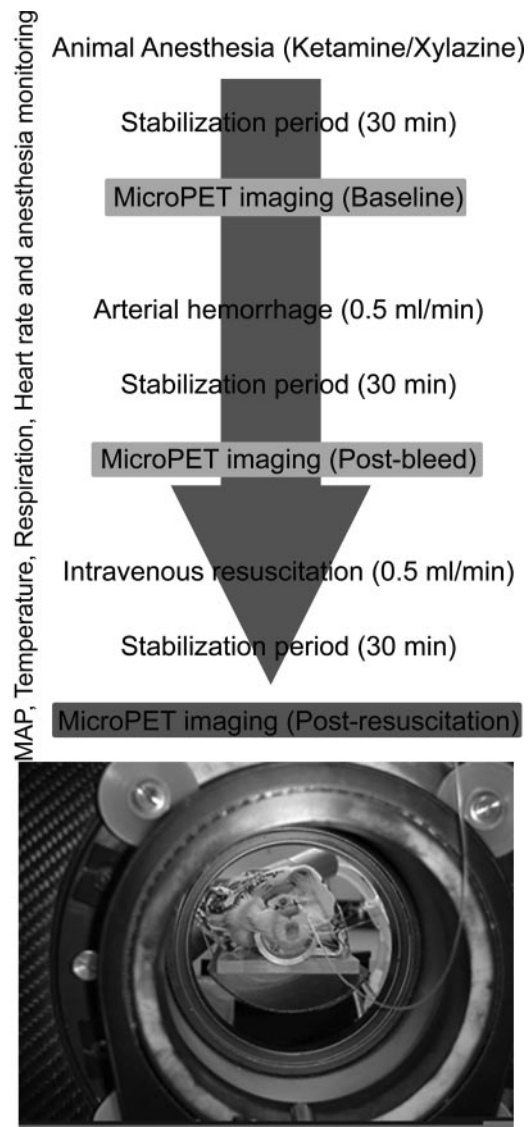


Fig. 2. *Top*: flow chart of micro-positron-emission tomography (micro-PET) imaging study in rats. Each animal is subjected to 3 imaging stages: baseline, postbleed, and postresuscitation. Blood pressure and rectal temperature were monitored through the entire study. MAP, mean arterial pressure. *Bottom*: rat wrapped in a warming blanket, instrumented, and positioned inside a micro-PET detector ring.

and a voxel size of  $0.85 \times 0.85 \times 1.21 \text{ mm}^3$  was reconstructed for each time frame using a two-dimensional (2-D) filtered back-projection algorithm. A ramp filter (cut-off frequency, 0.5/pixel) was used in the transverse plane (matrix size  $128 \times 128$ ), and a Hanning filter (cut-off frequency, 0.5/pixel) was used along the axial direction (63 slices). Decay and dead time corrections were automatically performed during the reconstruction process. Arterial input function (AIF) was determined by a method developed by Yee et al. (65). The method is based on drawing a region of interest (ROI) over the ventricular space of cardiac image and using a mathematical algorithm (65, 66) to derive input function that is not contaminated by signal from surrounding tissue (see APPENDIX A).

**Data analysis.** To calculate  $\text{CMR}_{\text{O}_2}$ , a mathematical algorithm developed by Ohta et al. was used (31, 64). The compartment model used by Ohta is described in APPENDIX B (see Fig. 7). This method needs only one scan from single-bolus  $^{15}\text{O}$ -labeled  $\text{O}_2$  inhalation and

was especially useful in the study of an animal model of hemorrhagic shock. The one-step computation utilizes a time-weighted integral method using three weighting functions to determine unknown variables (2, 8, 17, 56). The mathematical algorithm for solutions to Ohta's model was developed by Dr. Yee in MATLAB (The MathWorks, Natick, MA). The theoretical basis of Ohta's model is explained in APPENDIX B.

**Statistical analysis.** The data were analyzed for significant difference ( $P < 0.05$ ) by ANOVA using Prism software (GraphPad). Mean arterial pressure (MAP) was calculated by adding one-third of the pulse pressure to the diastolic pressure.

## RESULTS

In this work, we utilized  $^{15}\text{O}$ -micro-PET imaging to determine cerebral oxygen metabolism in a rat model of hemorrhagic shock. We evaluated the capacity of LEH to improve  $\text{CMR}_{\text{O}_2}$  and also compared the performance of LEH with saline and 5% HSA as control resuscitation fluids. LEH formulation consisted of neutral lipids containing  $\sim 7.5\%$  Hb (Table 1).

**LEH delivers  $^{15}\text{O}$ -labeled oxygen to cerebral tissue.** In the initial phase of this study, we demonstrated that LEH is capable of carrying oxygen. Figure 3 shows a set of cerebral micro-PET images of a rat injected with  $^{15}\text{O}$ -labeled LEH. As a comparison, a similarly processed  $^{15}\text{O}$ -labeled rat RBC preparation was also injected in an identical fashion. It is clear from the images that LEH is capable of transporting oxygen *in vivo* and delivers it to the cerebral tissue in a manner similar to that of RBCs. When oxygen gas was replaced by  $^{15}\text{O}$ -labeled carbon monoxide, both RBC and LEH avidly picked up  $\text{C}^{15}\text{O}$ . On intravenous injection,  $\text{C}^{15}\text{O}$ -labeled RBCs showed typical distribution of carbonylated RBCs where very little  $\text{C}^{15}\text{O}$  is released from the RBCs. The  $\text{C}^{15}\text{O}$ -RBC image was characterized by insignificant  $^{15}\text{O}$  activity in the cerebral tissue, and the majority of activity remained in the vascular pool. Carotid arteries could be clearly visualized in the  $\text{C}^{15}\text{O}$ -labeled RBC scan.

**LEH improves cerebral oxygen metabolism.** We followed the initial imaging studies with  $^{15}\text{O}$ -micro-PET investigations to monitor the performance of LEH in improving cerebral metabolism of oxygen in a rat model of 40% hemorrhage. Through the entire study, animals were kept anesthetized, and their vital signs were noted periodically. Core body temperature was successfully maintained at  $37 \pm 1^\circ\text{C}$  by using a warm water blanket. Figure 4A shows hematocrit in animals subjected to hypovolemia and resuscitation. After blood withdrawal, hematocrit decreased to a level consistent with the extent of loss. There was no significant difference in the values

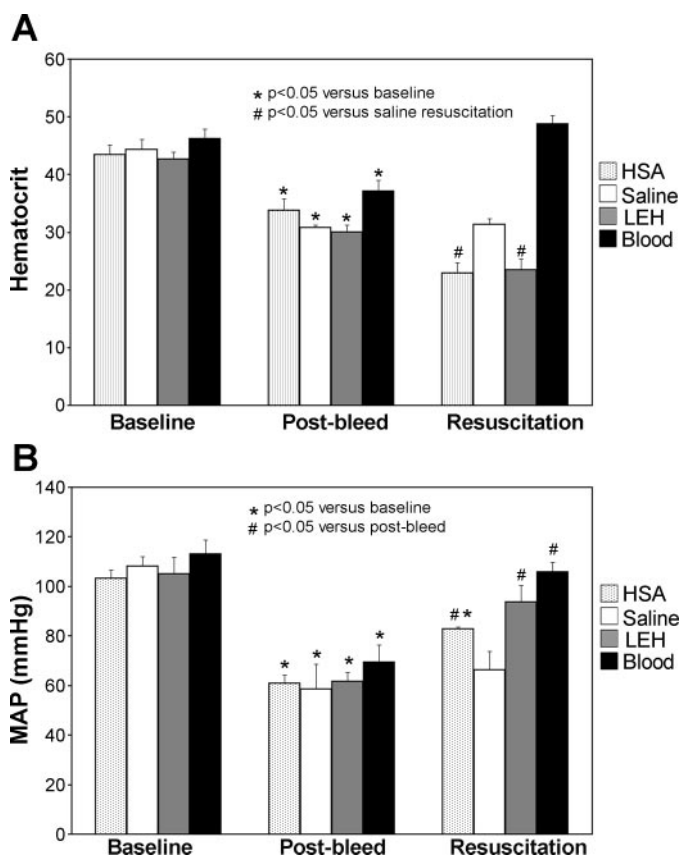


Fig. 4. Hematocrit (A) and MAP (B) in rats subjected to 40% hemorrhage followed by resuscitation with one of the test fluids. HSA, human serum albumin.

of hematocrit in the groups at baseline and postbleed stages. After resuscitation with HSA and LEH, hematocrit of animals decreased further, perhaps reflecting the hemodilution effect of HSA-induced plasma expansion. No such effect was observed in the animals that were resuscitated with saline, suggesting that saline rapidly equilibrates with interstitial fluid, which results in loss of vascular volume. Resuscitation with shed blood brought hematocrit to the baseline level. The difference in the hematocrits of animals belonging to HAS-containing fluids (5% HSA and LEH) and the saline group was statistically significant ( $P < 0.05$ ). The supernatant in the hematocrit tube after centrifugation of samples from LEH-resuscitated animals showed the presence of LEH in plasma.

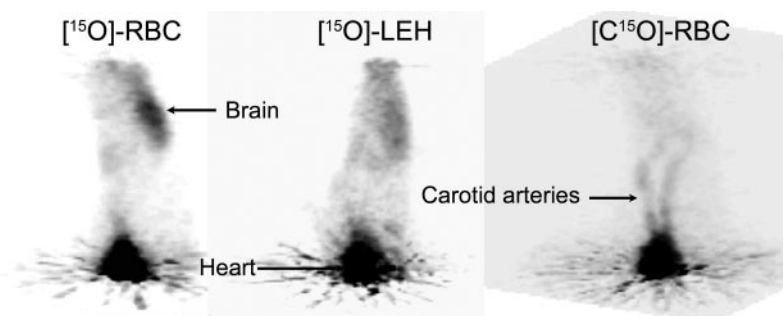


Fig. 3. Images of rat brain intravenously injected with red blood cells (RBCs) or LEH, both labeled with  $^{15}\text{O}$  tracers. Hb content of injected LEH was approximately one-half of that in RBCs. There is negligible tissue  $^{15}\text{O}$  activity when RBCs are in carbonylated form. Approximate dose of labeled preparations was  $^{15}\text{O}_2\text{-RBC} = 0.5 \text{ mCi}$ ,  $^{15}\text{O}_2\text{-LEH} = 0.2 \text{ mCi}$ , and  $\text{C}^{15}\text{O-RBC} = 0.2 \mu\text{Ci}$ .

Figure 4B shows the changes in MAP in animals with hemorrhagic shock and resuscitation. After induction of hypovolemia, MAP decreased in correlation with the amount of blood loss. The MAP values at baseline and after hemorrhage were not significantly different among various groups. Saline resuscitation improved MAP only marginally, but 5% HSA was able to partially recover blood pressure to  $\sim 80\%$  of baseline level. On the other hand, LEH suspended in 5% HSA consistently improved MAP to  $\sim 90\%$  of baseline blood pressure. The outcome was reflective of the capacity of these fluids to expand plasma. At the same time, the difference between the HSA and LEH groups appears to be a result of LEH's ability to transport oxygen. Obviously, shed blood was the best-performing fluid among the fluids tested. The results demonstrate the utility of having an oxygen carrier contained within plasma expanding resuscitation fluids for treatment of acute hemorrhagic shock. Perhaps the capacity to transport oxygen subdues physiological feedback mechanisms in response to acute blood loss.

Figure 5A shows the micro-PET images of a rat that was insufflated with 5 ml of 1 mCi  $^{15}\text{O}$ -labeled oxygen gas. The image set depicts a baseline scenario in the rat model. Both cardiac space and cerebral tissue was easily included within the field of view of the detector. The images were analyzed by drawing 3-D ROIs over brain and cardiac ventricular space. Transaxial and sagittal sections were used to draw brain and cardiac ROIs, respectively. The time-activity curves (TACs) generated from the ROIs are included in Fig. 5B. The heart curve showed a typical input curve characterized by a rapid rise to the peak followed by a quick distribution of  $^{15}\text{O}$

activity. The brain curve, on the other hand, attained a short plateau relatively slowly. The cerebral activity decreased as  $^{15}\text{O}$ -labeled  $\text{O}_2$  is metabolized to  $^{15}\text{O}$ -labeled water, which equilibrates with the vascular space. The portions of the curve beyond the 150-s time period are characterized by considerable noise. This data noise is more pronounced in the cardiac curve. It is a result of difficulty in selecting pure arterial space in a moving cardiac target, especially when rebinning is performed at 1 s/frame. Another reason is the rapid distribution and decay of  $^{15}\text{O}$  activity (physical decay  $T_{1/2} = 2$  min).

The TAC data were used to calculate  $\text{CMR}_{\text{O}_2}$  in a MATLAB program based on Ohta's model (31) as described in APPENDIX B. It is clear from Fig. 6 that both saline and 5% HSA perform poorly in restoring  $\text{CMR}_{\text{O}_2}$  to its baseline value. LEH resuscitation, however, was able to recover  $\text{CMR}_{\text{O}_2}$  to  $\sim 80\%$  of the baseline  $\text{CMR}_{\text{O}_2}$ . The improvement was statistically significant from both the baseline value as well as the post-resuscitation  $\text{CMR}_{\text{O}_2}$  value in saline and HSA groups ( $P < 0.05$ ). When animals were resuscitated with shed blood,  $\text{CMR}_{\text{O}_2}$  improved to more than baseline level. From these results it is evident that LEH is capable of transporting oxygen to the tissues. It delivers oxygen in a form and manner that is of benefit in improving oxygen metabolism. However, it does not match the efficacy of fresh shed blood in restoring oxygen metabolism. This is the first study of its kind to demonstrate in vivo efficacy of an artificial oxygen carrier in improving cerebral oxygen metabolism in a hemorrhagic shock model. It also highlights the technology of

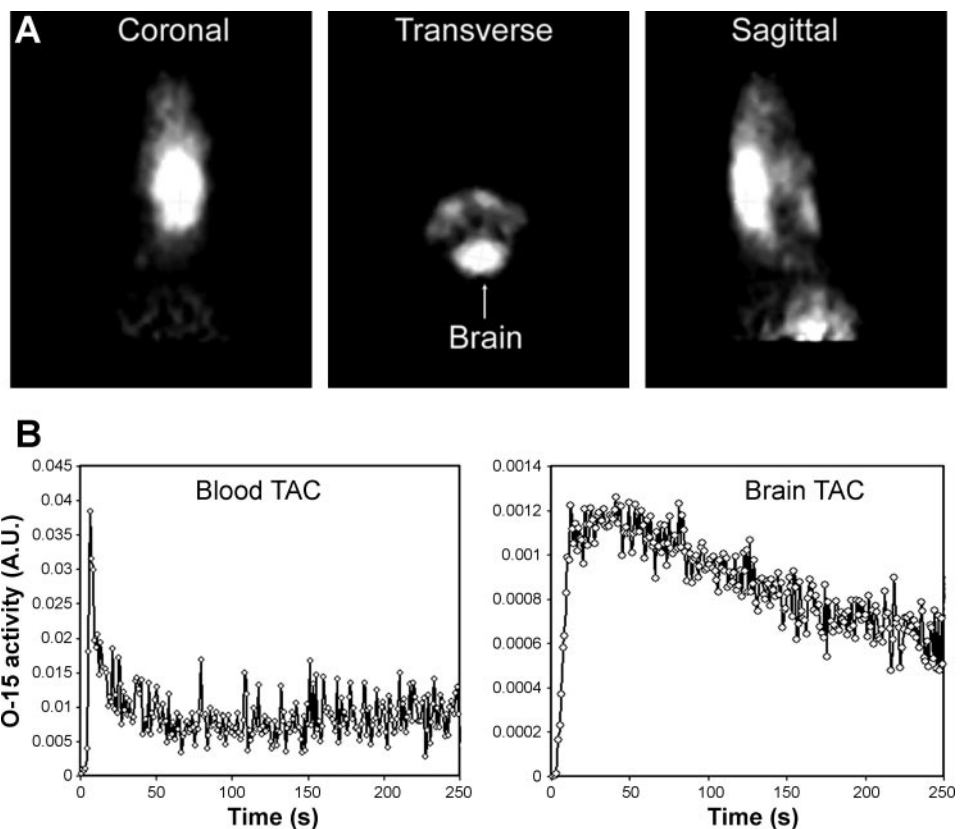


Fig. 5. A: summed micro-PET images of an LEH-resuscitated rat insufflated with  $\sim 1$  mCi of  $^{15}\text{O}$ -labeled  $\text{O}_2$  gas. The images clearly show that both brain and heart can be imaged together in the field of view. B: time-activity curves (TAC) obtained by drawing 3-dimensional regions of interest around cardiac ventricular space and the cerebral tissue in images rebinned at 1 s/frame. The cardiac TAC was used to derive arterial input function for cerebral metabolic rate of  $\text{O}_2$   $\text{CMR}_{\text{O}_2}$  estimations.

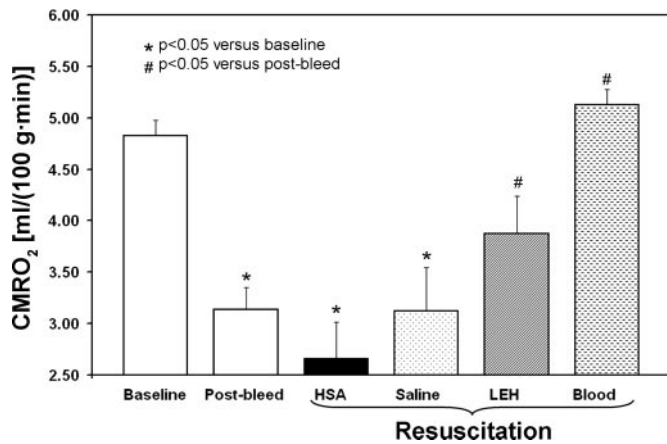


Fig. 6. CMRO<sub>2</sub> in rats subjected to 40% hemorrhage followed by resuscitation with test fluids. LEH was compared with saline, 5% HSA, and shed blood for improvement in CMRO<sub>2</sub>.

<sup>15</sup>O-PET imaging to directly investigate purported physiological effects of other blood substitutes or oxygen carriers.

## DISCUSSION

In healthy adults, resting oxygen delivery (DO<sub>2</sub>) is ~1 l/min. Tissues extract ~25% of delivered oxygen, leaving 75% of O<sub>2</sub> in the venous blood as an oxygen reserve. Up to a certain point, if DO<sub>2</sub> decreases, oxygen extraction ratio (OER) increases, so that oxygen consumption is maintained essentially constant. However, the extent of this relationship varies from tissue to tissue and depends on the magnitude of hypoxia. For example, in severely hypoxic brain, the OER increase is incapable of compensating for the delivery deficit, which results in reduced oxygen consumption. When blood loss outpaces the physiological adaptive mechanisms, resuscitation with oxygen carriers becomes necessary to maintain appropriate oxygen delivery. Mathematically, DO<sub>2</sub> is a product of cardiac output and arterial oxygen content (CaO<sub>2</sub>). Therefore, tissue oxygen delivery can be enhanced by increasing either cardiac output (9) or CaO<sub>2</sub>. However, beyond a certain point, increasing cardiac output actually worsens the shock status. Therefore, more attention is being given to enhancing CaO<sub>2</sub> by improving oxygen-carrying capacity. Development of artificial oxygen carriers is an effort in this direction.

LEH contains highly concentrated (>36 g/dl) purified Hb within the phospholipid membranes, usually composed of a saturated phosphatidylcholine, cholesterol, and 5–10% of an anionic lipid. Anionic lipids enhance Hb encapsulation, but they are also known to induce toxic reactions (32, 48–50). These reactions can be partially mitigated by incorporating PEG-linked lipids (55). We have developed a neutral PEG-linked-LEH (PEG-LEH) of homogeneous particle size (200–250 nm), with large Hb load and long circulation T<sub>1/2</sub> (3, 4). Using advanced manufacturing techniques for size reduction, endotoxin elimination, and PEGylation, the current preparation of LEH is less likely to induce reactions that are collectively called complement activation-related pseudoallergy (CARPA) (32, 48–50). Moreover, by adding HSA in the external medium, it is possible to formulate LEH as an oncotic, oxygen-carrying fluid. We have also observed in vitro that the presence

of catalase and certain oxidoreductive cofactors from RBCs improve shelf stability of Hb against autoxidation (unpublished data). This observation is supported by reports from other groups (30, 51, 53).

Several factors, such as lipid composition, size, PEGylation, oxygen affinity, viscosity, oncotic activity, and isotonicity, affect the in vivo efficacy of LEH. Using nuclear imaging and biodistribution studies, we have shown that liver and spleen are the major organs of LEH accumulation (3, 4). The uptake of LEH by RES is also dependent on the amount administered (23). A large dose of liposomes saturates the endocytotic elimination pathways or depletes the plasma opsonizing factors and tends to increase the circulating liposomes in blood (12). Administration of large amounts of LEH does not cause any irreversible damage to the RES (40, 41). It is also desirable that the intravascular persistence of LEH be at least equal to the time required to regenerate RBCs (43). Following blood loss, the lost blood volume and oxygen-carrying capacity is replaced in 5–7 days (18). Our PEG-LEH preparation has a circulation T<sub>1/2</sub> of 30 and 39 h, respectively, in rats and rabbits with 25% hypovolemic shock (3, 4). LEH T<sub>1/2</sub> of 30 h in rats roughly translates to ~90 h in humans (63).

LEH, as well as other Hb-based oxygen carriers (HBOCs), have undergone extensive preclinical evaluation in animal models of hemorrhagic shock. The successful transition of these products from preclinical to clinical stages has been based on the assessment of surrogate markers after resuscitation. While a few HBOCs have already entered clinical trials, actual improvement in cerebral oxygen delivery and metabolism after their administration has not been demonstrated. An efficient oxygen carrier is not necessarily an efficient oxygen-delivery vehicle, and an effective delivery in turn may not always result in improved oxygen metabolism. Thus, if replenishing oxygen delivery is the prime objective of resuscitation, monitoring oxygen delivery, oxygen consumption, and local tissue acidosis is of primary significance. While tissue acidosis has serum markers, lactate and base deficit, procedures that may provide a direct measurement of tissue oxygenation are too invasive (60). Several techniques, such as near-infrared spectroscopy (NIRS) (59), polarographic electrode placement (24), and other invasive techniques (10), have been used to monitor tissue oxygen. NIRS is easy and noninvasive, but it has been found to lack correlation with standard technique of jugular venous oxygen saturation (52). Second, since this technique is based on the differential absorption spectra of Hb, oxy-Hb, and cytochrome oxidase, it is not clear how useful NIRS can be in assessing oxygen metabolism and evaluation of HBOCs. With other sparingly used techniques, the true meaning of the alteration in signals generated by these techniques has not been correlated with specific functional state of the tissue (45).

Several other groups of investigators have used indirect techniques of measurement and have shown that LEH is capable of correcting oxygen deficit in peripheral tissues (20, 34, 42, 67). In this work we demonstrate that PET has the capability to visually, quantitatively, and noninvasively assess oxygen delivery and metabolism in live animals for the functional evaluation of resuscitation with HBOCs. CMRO<sub>2</sub> is quantified as a product of cerebral blood flow (CBF), OER, and CaO<sub>2</sub>. Because oxygen transport across membranes follows

passive diffusion, intracellular oxygen tension ( $P_{iO_2}$ ) is driven by the brain oxygen tension ( $P_{br O_2}$ ), which in turn is directly related to  $Ca_{O_2}$ . After hemorrhagic shock,  $P_{br O_2}$  may decrease from a normal level of 35 mmHg to below a critical level of 15–20 mmHg (16, 22, 68). In mild blood loss,  $P_{br O_2}$  is maintained above the critical level by cerebral autoregulation. Autoregulation is helpful only within a MAP of 60–150 mmHg because the diffusion force to deliver oxygen to mitochondria is drastically reduced in severe hemorrhage (68). The diffusion distance for oxygen from the microvasculature also increases because of tissue edema and damage resulting from the hemorrhage. Because of the altered diffusivity and cerebral autoregulation, exclusive assessment of  $Ca_{O_2}$  or  $P_{br O_2}$  alone may not be sufficient, and additional information about cerebral oxygen metabolism and energy metabolism is necessary (68). As illustrated in Fig. 1, increased  $Ca_{O_2}$  may not necessarily result in enhanced  $P_{br O_2}$  and higher  $P_{br O_2}$  may not necessarily mean higher  $P_{iO_2}$ .  $CMR_{O_2}$  is the best predictor of reversible or irreversible brain damage. A drop in oxygen metabolism below 61–69% of the basal level is deemed critical (13). Thus information obtained from parametric PET images of  $CMR_{O_2}$  (28) may be used to predict the reversibility of brain damage.

We applied  $^{15}O$ -PET imaging to investigate the capacity of LEH to deliver oxygen. We used Ohta's simplified two-compartment model, which eliminated the need to determine cerebral blood flow and volume for accurate estimation of  $CMR_{O_2}$ . The procedure was further made less complicated by the use of cardiac arterial space to derive AIF as described in APPENDIX A. With regard to the improvement in  $CMR_{O_2}$ , LEH performed significantly better than the control fluids containing no oxygen-carrying capability. However, in comparison, whole blood was the most efficient fluid in restoring  $CMR_{O_2}$  to its baseline level. At this point, it should be noted that LEH contained about one-half the amount of Hb present in shed blood. LEH has relatively large dimensions compared with the molecularly modified Hbs (39) but is very small compared with RBCs. It is possible that the small size of LEH helps it distribute more homogeneously in the vascular space compared with RBCs, which in turn helps in improving oxygen delivery of LEH relative to its Hb content. Further study with matching Hb concentrations in LEH and shed blood is required to establish bioequivalency.

A correction in volume deficit at the cardiovascular level may not necessarily mean recovery of cellular oxygen metabolism. Both HSA and LEH significantly improved MAP by virtue of their oncotic activity, but only LEH helped in restitution of  $CMR_{O_2}$  to a significant level. Besides being not capable of carrying oxygen, HSA also has a tendency to dilute hematocrit by pulling interstitial water to balance the hydrostatic pressure in the vessels. On the other hand, isoncotic saline has no such propensity of hemodilution. In a victim of acute blood loss, infusion of normal saline leads to edema, because in the absence of any significant oncotic pressure, the fluid leaks into extracellular space along hydrostatic pressure. The present formulation of LEH is oncotic by virtue of 5% HSA and is capable of enhancing arterial  $P_{O_2}$ , which is the driving force for passive diffusion of oxygen into the tissue. More detailed study encompassing the evaluation of cerebral blood flow and cerebral blood volume is required to appropri-

ately assess hemodynamic reserve in response to resuscitation with HSA and LEH.

In summary, this report demonstrates that LEH resuscitation is capable of improving  $CMR_{O_2}$  by efficiently delivering oxygen to the hypoxic cerebral tissue. It would be of interest to compare LEH performance with whole blood resuscitation when the Hb content of both fluids is matched. The unique ability of  $^{15}O$ -PET to physiologically quantify metabolic rate in critical organs has been applied for the first time to evaluate artificial oxygen carriers. It is anticipated that this novel PET technology will be further utilized as a global approach to assess various other Hb-based oxygen carriers that are in various stages of clinical trials. Utility of PET is not limited to the evaluation of oxygen metabolism only. PET investigation of oxygen metabolism may also enable us to differentiate between the mechanisms with which HBOCs improve shock status. For instance, molecularly modified Hbs, such as Oxyglobin, are capable not only of transporting oxygen but also of increasing the intravascular oncotic pressure (58). At present, it is unclear whether HBOCs improve shock status because of the oxygen carriage or the oncotic activity. Rapid oxidation of free Hb diminishes the oxygen-carrying ability of HBOCs, but its oncotic activity is still mostly preserved. It is possible that the initial beneficial effect of the molecularly modified Hbs may be due to both mechanisms, while at later times, oncotic activity prevails. By a simultaneous determination of circulating amount, ability to carry oxygen, and improvement in  $CMR_{O_2}$ , it may be possible to delineate the mechanism of action of HBOCs.

#### APPENDIX A

##### *Image-Derived AIF*

Quantitative PET to study metabolism is strictly dependent on an accurate AIF. One way to derive AIF is to frequently sample arterial blood to measure instantaneous radiotracer concentration with respect to time. In humans, large blood volume, an accessible arterial space, and a reduced sampling frequency enable investigators to perform external blood sampling to determine AIF with relative ease. In small animals, such as rats, limited blood volume and rapid blood turnover necessitates that a small volume ( $\leq 25 \mu\text{l}$ ) and rapid sampling (every 2–3 s) is done to derive arterial input function (7). With available technology, this is not possible without altering the underlying physiology of the animal model used in this study. Small blood volume, inaccessibility to arterial blood, and possibility of compromising normal physiology of animal model are a few of the major limitations in small animal PET. To circumvent this problem, Yee et al. (65) reported a noninvasive method of obtaining AIF by drawing a ROI over cardiac ventricular space in the image. The method is based on the assumption that the TAC obtained in an ROI drawn over the heart would closely approximate actual AIF. We have validated this technique in a rat model against a standard method of external blood sampling (unpublished work). This approach has been successfully applied in the case of humans (19). However, in small animals, the cardiac TAC will always be contaminated with input from surrounding myocardial tissue. Partial volume effect and continuous heart motion make it impossible to draw an ROI that covers

pure ventricular space. Yee et al. derived a mathematical algorithm to nullify the impact of extraventricular contribution in TAC by considering that any volume covered by an ROI ( $V_{ROI}$ ) is a sum of real volume of arterial space ( $V_a$ ) and the volume of myocardial space included in the ROI ( $V_m$ ).

$$V_{ROI} = V_a + V_m \quad (A1)$$

The above equation may be rearranged by using respective concentration terms to arrive at Eq. A2

$$C_a = C_{ROI} + C_{ROI} \cdot \left[ \frac{V_m}{V_a} \left( 1 - \frac{C_m}{C_{ROI}} \right) \right] \quad (A2)$$

where  $C_a$ ,  $C_{ROI}$ , and  $C_m$  are the concentration in arterial space, ROI, and myocardial space, respectively. In Eq. A2, the second term in the right is nothing but an error that needs to be added to the data obtained from nonideal ROI to derive the real concentration,  $C_a$ . Immediately after tracer injection (i.e.,  $t = 0$ ), the value of  $C_m$  is zero, and after some time when the tracer has equilibrated within myocardial tissue and arterial blood,  $C_m$  is equal to  $C_{ROI}$ . Assuming that the transition of  $C_m$  from 0 to  $C_{ROI}$  is asymptotic, actual AIF can be obtained from the measured TAC of the ROI by introducing a correction function  $D(t)$ . The value of function  $D(t)$  decays from  $V_m/V_a$  ( $t = 0$ ) to 0 ( $t = \infty$ ). Reframing Eq. A2, true AIF [ $S_a(t)$ ] may be derived from nonideal AIF [ $S_{ROI}(t)$ ] by using Eq. A3:

$$S_a(t) = S_{ROI}(t) + S_{ROI}(t) \cdot D(t) \quad (A3)$$

where  $D(t)$  exponentially decays from its initial value  $D_0 = V_m/V_a$  with a half-life,  $T$  (Eq. A4)

$$D(t) = D_0 \cdot \exp\left(-\frac{0.693}{T} \cdot t\right) \quad (A4)$$

This approach has been discussed in detail elsewhere (65, 66).

#### APPENDIX B

##### Mathematical Basis of $CMR_{O_2}$ Calculation

On the basis of Ohta's model, oxygen metabolism is predicted as a product of unidirectional clearance parameter from blood to brain  $K_1^{O_2}$  and arterial tracer concentration  $C_a^{O_2}$  (Fig. 7). The parameter  $K_1^{O_2}$  can be determined independently of the rate of efflux of tracer from the brain tissue, and the recirculating water does not influence its estimation significantly (31). While  $C_a^{O_2}$  may be easily determined by a blood sample, the problem of  $K_1^{O_2}$  estimation demands a relatively complex weighted integration mode (2, 31). The approach corrects the estimation for recirculating tracer, differing tracer partition coefficients, and residual radioactivity in the circulation. In association with Fig. 7, the technique may be depicted by Eq. B1

$$M(t) = K_1^{O_2} \int_0^t C_a(u) \exp[k_2^{O_2}(u-t)] du + V_0 C_a(t) \quad (B1)$$

In Eq. B1,  $M(t)$  is the total  $^{15}O$  activity in the PET image at time  $t$ ,  $K_1^{O_2}$  is the clearance of tracer from arterial blood,  $k_2^{O_2}$  is

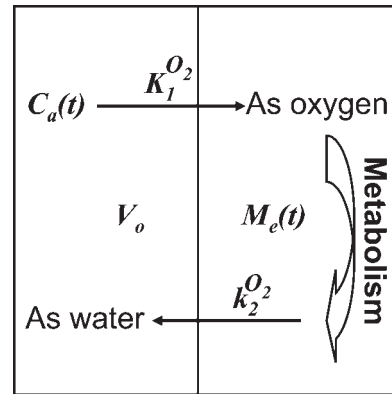


Fig. 7. A model configuration for the calculation of  $CMR_{O_2}$ . In the model,  $M_e(t)$  is the total  $^{15}O$  activity in the PET image,  $V_o$  is the vascular volume,  $K_1^{O_2}$  is the clearance of tracer,  $k_2^{O_2}$  is the washout rate of metabolized water from brain to blood, and  $C_a(t)$  is the total arterial  $^{15}O$  activity.

the washout rate of metabolized water from brain to blood,  $V_o$  is the volume factor related to the cerebral blood volume (CBV), and  $C_a(t)$  is the total arterial  $^{15}O$  activity. Alternatively, the three unknowns in Eq. B1 may be described as

$$K_1^{O_2} = CBF \times \text{oxygen extraction fraction}$$

$$k_2^{O_2} = CBF/\lambda$$

where  $\lambda$  is brain-blood partition coefficient of water; and

$$V_o = CBV$$

These parameters can be determined by a time-weighted integral method. When both sides of Eq. B1 are successively multiplied by weighting functions  $w_1(t)$ ,  $w_2(t)$ , and  $w_3(t)$ , the following equations emerge:

$$\int_0^T w_1(t)M(t)dt = K_1^{O_2} \int_0^T w_1(t) \int_0^t C_a(u) \exp[k_2^{O_2}(u-t)] du dt + V_0 \int_0^T w_1(t) C_a(t) dt \quad (B2)$$

$$\int_0^T w_2(t)M(t)dt = K_1^{O_2} \int_0^T w_2(t) \int_0^t C_a(u) \exp[k_2^{O_2}(u-t)] du dt + V_0 \int_0^T w_2(t) C_a(t) dt \quad (B3)$$

$$\int_0^T w_3(t)M(t)dt = K_1^{O_2} \int_0^T w_3(t) \int_0^t C_a(u) \exp[k_2^{O_2}(u-t)] du dt + V_0 \int_0^T w_3(t) C_a(t) dt \quad (B4)$$

Rearranging Eqs. B2–B4 to eliminate  $V_0$  provides us with Eq. B5 for computation of  $k_2^{O_2}$ .

$$\begin{aligned}
& \frac{\int_0^T w_3(t)C_a(t)dt \cdot \int_0^T w_1(t)M(t)dt - \int_0^T w_1(t)C_a(t)dt \cdot \int_0^T w_3(t)M(t)dt}{\int_0^T w_3(t)C_a(t)dt \cdot \int_0^T w_2(t)M(t)dt - \int_0^T w_2(t)C_a(t)dt \cdot \int_0^T w_3(t)M(t)dt} \\
&= \frac{\int_0^T w_3(t)C_a(t)dt \cdot \int_0^T w_1(t) \int_0^t C_a(u) \exp[k_2^{O_2}(u-t)]du dt - \int_0^T w_1(t)C_a(t)dt \cdot \int_0^T w_3(t) \int_0^t C_a(u) \exp[k_2^{O_2}(u-t)]du dt}{\int_0^T w_3(t)C_a(t)dt \cdot \int_0^T w_2(t) \int_0^t C_a(u) \exp[k_2^{O_2}(u-t)]du dt - \int_0^T w_2(t)C_a(t)dt \cdot \int_0^T w_3(t) \int_0^t C_a(u) \exp[k_2^{O_2}(u-t)]du dt}
\end{aligned} \tag{B5}$$

Equation B5 is used to generate a look-up table of the right-hand side ratio for various values of  $k_2^{O_2}$ . The left-hand side of Eq. B5 is obtained from PET image analysis as integral cerebral tissue TAC,  $M(t)$ , and arterial input function  $C_a(t)$ . Since the 3-D analysis of images provides a measure of concentration per unit voxel volume,  $M(t)$  is multiplied by reciprocal of brain tissue density to obtain concentration per unit mass. Once  $k_2^{O_2}$  is known,  $K_1^{O_2}$  may be calculated using equations derived from rearrangement of Eqs. B2 and B4.

$$\begin{aligned}
K_1^{O_2} = & \frac{\int_0^T w_3(t)C_a(t)dt \cdot \int_0^T w_1(t)M(t)dt - \int_0^T w_1(t)C_a(t)dt \cdot \int_0^T w_3(t)M(t)dt}{\int_0^T w_3(t)C_a(t)dt \cdot \int_0^T w_1(t) \int_0^t C_a(u) \exp[k_2^{O_2}(u-t)]du dt - \int_0^T w_3(t)C_a(t)dt \cdot \int_0^T w_1(t) \int_0^t C_a(u) \exp[k_2^{O_2}(u-t)]du dt}
\end{aligned} \tag{B6}$$

Finally,  $CMR_{O_2}$  is calculated as a product of  $K_1^{O_2}$  and  $C_a^{O_2}$ , where  $C_a^{O_2}$  is the arterial oxygen content. In the model used in this work,  $w_1(t)$ ,  $w_2(t)$ , and  $w_3(t)$  were 1,  $t$ , and  $\sqrt{t}$ , respectively. The value of  $t$  is the time elapsed up to the image acquisition time, which progresses from 0 to 240 s in 1-s increments for a total imaging time of 6 min. All calculations were computed in a MATLAB environment.

#### ACKNOWLEDGMENTS

Technical help from Cristina Santoyo and Shiva Raidas is acknowledged.

#### GRANTS

This work was supported by Office of Naval Research (Washington DC) Grant N00140010793 and National Institute of Biomedical Imaging and Bioengineering/National Institutes of Health (Bethesda, MD) Grant EB005187-01A1.

#### REFERENCES

1. Ali AA, Ali GS, Steinke JM, Shepherd AP. Co-oximetry interference by hemoglobin-based blood substitutes. *Anesth Analg* 92: 863–869, 2001.
2. Alpert NM, Eriksson L, Chang JY, Bergstrom M, Litton JE, Correia JA, Bohm C, Ackerman RH, Taveras JM. Strategy for the measurement of regional cerebral blood flow using short-lived tracers and emission tomography. *J Cereb Blood Flow Metab* 4: 28–34, 1984.
3. Awasthi VD, Garcia D, Klipper R, Goins BA, Phillips WT. Neutral and anionic liposome-encapsulated hemoglobin: effect of postinserted poly-(ethylene glycol)-distearoylphosphatidylethanolamine on distribution and circulation kinetics. *J Pharmacol Exp Ther* 309: 241–248, 2004.
4. Awasthi VD, Garcia D, Klipper R, Phillips WT, Goins BA. Kinetics of liposome-encapsulated hemoglobin after 25% hypovolemic exchange transfusion. *Int J Pharm* 283: 53–62, 2004.
5. Baron BJ, Scalea TM. Acute blood loss. *Emerg Med Clin North Am* 14: 35–55, 1996.
6. Bellamy RF, Maningas PA, Wenger BA. Current shock models and clinical correlations. *Ann Emerg Med* 15: 1392–1395, 1986.
7. Bentourkia M. Kinetic modeling of PET data without blood sampling. *IEEE Trans Nucl Sci* 52: 697–702, 2005.
8. Carson RE, Huang SC, Green MV. Weighted integration method for local cerebral blood flow measurements with positron emission tomography. *J Cereb Blood Flow Metab* 6: 245–258, 1986.
9. Chernow B. New advances in the pharmacologic approach to circulatory shock. *J Clin Anesth* 8: 67S–69S, 1996.
10. Cruz J, Raps EC, Hoffstad OJ, Jaggi JL, Gennarelli TA. Cerebral oxygen monitoring. *Crit Care Med* 21: 1242–1246, 1993.
11. Deprise M, Kinahan PE, Townsend DW, Michel C, Sibomana M, Newport DF. Exact and approximate rebinning algorithms for 3-D PET data. *IEEE Trans Med Imaging* 16: 145–158, 1997.
12. Drummond DC, Meyer O, Hong K, Kirpotin DB, Papahadjopoulos D. Optimizing liposomes for delivery of chemotherapeutic agents to solid tumors. *Pharmacol Rev* 51: 691–743, 1999.
13. Frykholm P, Andersson JL, Valtysson J, Silander HC, Hillered L, Persson L, Olsson Y, Yu WR, Westerberg G, Watanabe Y, Langstrom B, Enblad P. A metabolic threshold of irreversible ischemia demonstrated by PET in a middle cerebral artery occlusion-reperfusion primate model. *Acta Neurol Scand* 102: 18–26, 2000.
14. Goins B, Klipper R, Sanders J, Cliff RO, Rudolph AS, Phillips WT. Physiological responses, organ distribution, and circulation kinetics in anesthetized rats after hypovolemic exchange transfusion with technetium-99m-labeled liposome-encapsulated hemoglobin. *Shock* 4: 121–130, 1995.
15. Hirschl RB. Oxygen delivery in the pediatric surgical patient. *Curr Opin Pediatr* 6: 341–347, 1994.
16. Hoffman WE, Charbel FT, Edelman G. Brain tissue oxygen, carbon dioxide, and pH in neurosurgical patients at risk for ischemia. *Anesth Analg* 82: 582–586, 1996.
17. Huang SC, Carson RE, Phelps ME. Measurement of local blood flow and distribution volume with short-lived isotopes: a general input technique. *J Cereb Blood Flow Metab* 2: 99–108, 1982.

18. Hughes GS Jr, Francome SF, Antal EJ, Adams WJ, Locker PK, Yancey EP, Jacobs EE Jr. Hematologic effects of a novel hemoglobin-based oxygen carrier in normal male and female subjects. *J Lab Clin Med* 126: 444–451, 1995.
19. Iida H, Miura S, Shoji Y, Ogawa T, Kado H, Narita Y, Hatazawa J, Eberl S, Kanno I, Uemura K. Noninvasive quantitation of cerebral blood flow using oxygen-15-water and a dual-PET system. *J Nucl Med* 39: 1789–1798, 1998.
20. Izumi Y, Sakai H, Kose T, Hamada K, Takeoka S, Yoshizu A, Horinouchi H, Kato R, Nishide H, Tsuchida E, Kobayashi K. Evaluation of the capabilities of a hemoglobin vesicle as an artificial oxygen carrier in a rat exchange transfusion model. *ASAIO J* 43: 289–297, 1997.
21. Kawano T, Hosoya H. Oxidative burst by acellular haemoglobin and neurotransmitters. *Med Hypotheses* 59: 11–15, 2002.
22. Kiening KL, Unterberg AW, Bardt TF, Schneider GH, Lanksch WR. Monitoring of cerebral oxygenation in patients with severe head injuries: brain tissue PO<sub>2</sub> versus jugular vein oxygen saturation. *J Neurosurg* 85: 751–757, 1996.
23. Laverman P, Brouwers AH, Dams ET, Oyen WJ, Storm G, van Rooijen N, Corstens FH, Boerman OC. Preclinical and clinical evidence for disappearance of long-circulating characteristics of polyethylene glycol liposomes at low lipid dose. *J Pharmacol Exp Ther* 293: 996–1001, 2000.
24. Manley GT, Pitts LH, Morabito D, Doyle CA, Gibson J, Gimbel M, Hopf HW, Knudson MM. Brain tissue oxygenation during hemorrhagic shock, resuscitation, and alterations in ventilation. *J Trauma* 46: 261–267, 1999.
25. Matej S, Karp JS, Lewitt RM, Becher AJ. Performance of the Fourier rebinning algorithm for PET with large acceptance angles. *Phys Med Biol* 43: 787–795, 1998.
26. Matsuoka T. Determination of methemoglobin and carboxyhemoglobin in blood by rapid colorimetry. *Biol Pharm Bull* 20: 1208–1211, 1997.
27. Mink RB, Pollack MM. Effect of blood transfusion on oxygen consumption in pediatric septic shock. *Crit Care Med* 18: 1087–1091, 1990.
28. Mintun MA, Raichle ME, Martin WR, Herscovitch P. Brain oxygen utilization measured with O-15 radiotracers and positron emission tomography. *J Nucl Med* 25: 177–187, 1984.
29. Nakai K, Matsuda N, Amano M, Ohta T, Tokuyama S, Akama K, Kawakami Y, Tsuchida E, Sekiguchi S. Acellular and cellular hemoglobin solutions as vasoconstrictive factor. *Artif Cells Blood Substit Immobil Biotechnol* 22: 559–564, 1994.
30. Ogata Y, Goto H, Kimura T, Fukui H. Development of neo red cells (NRC) with the enzymatic reduction system of methemoglobin. *Artif Cells Blood Substit Immobil Biotechnol* 25: 417–427, 1997.
31. Ohta S, Meyer E, Thompson CJ, Gjedde A. Oxygen consumption of the living human brain measured after a single inhalation of positron emitting oxygen. *J Cereb Blood Flow Metab* 12: 179–192, 1992.
32. Phillips WT, Klipper R, Fresne D, Rudolph AS, Javors M, Goins B. Platelet reactivity with liposome-encapsulated hemoglobin in the rat. *Exp Hematol* 25: 1347–1356, 1997.
33. Phillips WT, Klipper RW, Awasthi VD, Rudolph AS, Cliff R, Kwabisorski V, Goins BA. Polyethylene glycol-modified liposome-encapsulated hemoglobin: a long circulating red cell substitute. *J Pharmacol Exp Ther* 288: 665–670, 1999.
34. Plock JA, Contaldo C, Sakai H, Tsuchida E, Leunig M, Banic A, Menger MD, Erni D. Is hemoglobin in hemoglobin vesicles infused for isovolemic hemodilution necessary to improve oxygenation in critically ischemic hamster skin? *Am J Physiol Heart Circ Physiol* 289: H2624–H2631, 2005.
35. Rasmussen GE, Grande CM. Blood, fluids, and electrolytes in the pediatric trauma patient. *Int Anesthesiol Clin* 32: 79–101, 1994.
36. Rudolph AS. Encapsulation of hemoglobin in liposomes. In: *Blood Substitutes: Physiological Basis of Efficacy*, edited by Winslow RM, Vandegriff KD, Intaglietta M. Boston, MA: Birkhauser, 1995, p. 90–104.
37. Rudolph AS, Sulpizio A, Hieble P, MacDonald V, Chavez M, Feuerstein G. Liposome encapsulation attenuates hemoglobin-induced vasoconstriction in rabbit arterial segments. *J Appl Physiol* 82: 1826–1835, 1997.
38. Sakai H, Hamada K, Takeoka S, Nishide H, Tsuchida E. Physical properties of hemoglobin vesicles as red cell substitutes. *Biotechnol Prog* 12: 119–125, 1996.
39. Sakai H, Hara H, Yuasa M, Tsai AG, Takeoka S, Tsuchida E, Intaglietta M. Molecular dimensions of Hb-based O<sub>2</sub> carriers determine constriction of resistance arteries and hypertension. *Am J Physiol Heart Circ Physiol* 279: H908–H915, 2000.
40. Sakai H, Horinouchi H, Masada Y, Takeoka S, Ikeda E, Takaori M, Kobayashi K, Tsuchida E. Metabolism of hemoglobin-vesicles (artificial oxygen carriers) and their influence on organ functions in a rat model. *Biomaterials* 25: 4317–4325, 2004.
41. Sakai H, Horinouchi H, Tomiyama K, Ikeda E, Takeoka S, Kobayashi K, Tsuchida E. Hemoglobin-vesicles as oxygen carriers: influence on phagocytic activity and histopathological changes in reticuloendothelial system. *Am J Pathol* 159: 1079–1088, 2001.
42. Sakai H, Takeoka S, Wettstein R, Tsai AG, Intaglietta M, Tsuchida E. Systemic and microvascular responses to hemorrhagic shock and resuscitation with Hb vesicles. *Am J Physiol Heart Circ Physiol* 283: H1191–H1199, 2002.
43. Sehgal LR, Gould SA, Rosen AL, Sehgal HL, Moss GS. Polymerized pyridoxylated hemoglobin: a red cell substitute with normal oxygen capacity. *Surgery* 95: 433–438, 1984.
44. Sou K, Endo T, Takeoka S, Tsuchida E. Poly(ethylene glycol)-modification of the phospholipid vesicles by using the spontaneous incorporation of poly(ethylene glycol)-lipid into the vesicles. *Bioconjug Chem* 11: 372–379, 2000.
45. Spahn DR. Monitoring of oxygen delivery in cardiac and vascular surgery. *Vox Sang* 74, Suppl 2: 395–397, 1998.
46. Stewart JCM. Colorimetric determination of phospholipids with ammonium ferrioxalate. *Anal Biochem* 104: 10–14, 1980.
47. Stowell CP. Hemoglobin-based oxygen carriers. *Curr Opin Hematol* 9: 537–543, 2002.
48. Szebeni J. The interaction of liposomes with the complement system. *Crit Rev Ther Drug Carrier Syst* 15: 57–88, 1998.
49. Szebeni J, Baranyi L, Savay S, Bodo M, Morse DS, Basta M, Stahl GL, Bunger R, Alving CR. Liposome-induced pulmonary hypertension: properties and mechanism of a complement-mediated pseudoallergic reaction. *Am J Physiol Heart Circ Physiol* 279: H1319–H1328, 2000.
50. Szebeni J, Baranyi L, Savay S, Gotze O, Alving CR, Bunger R, Mongan PD. Complement activation during hemorrhagic shock and resuscitation in swine. *Shock* 20: 347–355, 2003.
51. Takeoka S, Sakai H, Kose T, Mano Y, Seino Y, Nishide H, Tsuchida E. Methemoglobin formation in hemoglobin vesicles and reduction by encapsulated thiols. *Bioconjug Chem* 8: 539–544, 1997.
52. Ter Minassian A, Poirier N, Pierrot M, Menei P, Granry JC, Ursino M, Beydon L. Correlation between cerebral oxygen saturation measured by near-infrared spectroscopy and jugular oxygen saturation in patients with severe closed head injury. *Anesthesiology* 91: 985–990, 1999.
53. Teramura Y, Kanazawa H, Sakai H, Takeoka S, Tsuchida E. Prolonged oxygen-carrying ability of hemoglobin vesicles by coencapsulation of catalase in vivo. *Bioconjug Chem* 14: 1171–1176, 2003.
54. Tomita S, Enoki Y, Santa M, Yoshida H, Yasumitsu Y. A simple spectrophotometric method for determination of met-hemoglobin in dilute solution. *J Nara Med Assoc* 19: 1–6, 1968.
55. Torchilin VP, Papisov MI. Why do polyethylene glycol-coated liposomes circulate so long? *J Liposome Res* 4: 725–739, 1994.
56. Tsui E, Budinger TF. Transverse section imaging of mean clearance time. *Phys Med Biol* 23: 644–653, 1978.
57. Usuba A, Motoki R. Safety and efficacy of encapsulated hemoglobin in hemorrhagic shock. In: *Artificial Red Cells: Materials, Performances and Clinical Study as Blood Substitutes*, edited by Tsuchida E. Chichester, UK: Wiley, 1995, p. 65–92.
58. Vandegriff KD, McCarthy M, Rohlfis RJ, Winslow RM. Colloid osmotic properties of modified hemoglobins: chemically cross-linked versus polyethylene glycol surface-conjugated. *Biophys Chem* 69: 23–30, 1997.
59. Wardle SP, Yoxall CW, Weindling AM. Determinants of cerebral fractional oxygen extraction using near infrared spectroscopy in preterm neonates. *J Cereb Blood Flow Metab* 20: 272–279, 2000.
60. Wilson M, Davis DP, Coimbra R. Diagnosis and monitoring of hemorrhagic shock during the initial resuscitation of multiple trauma patients: a review. *J Emerg Med* 24: 413–422, 2003.
61. Winslow RM. Current status of blood substitute research: towards a new paradigm. *J Intern Med* 253: 508–517, 2003.
62. Winslow RM, Chapman KW. Pilot-scale preparation of hemoglobin solutions. *Methods Enzymol* 231: 3–16, 1994.
63. Woodle MC, Newman MS, Working PK. Biological properties of sterically stabilized liposomes. In: *Stealth Liposomes*, edited by Lasic DD, Martin F. Boca Raton, FL: CRC Press, 1995, p. 103–117.
64. Yee SH, Jerabek P, Fox PT. Oxidative metabolic rate measurement of the rat brain using O<sup>15</sup>O microPET imaging. *Mol Imaging Biol* 6: 102, 2004.

65. **Yee SH, Jerabek PA, Fox PT.** Non-invasive quantification of cerebral blood flow for rats by microPET imaging of  $^{15}\text{O}$  labelled water: the application of a cardiac time-activity curve for the tracer arterial input function. *Nucl Med Commun* 26: 903–911, 2005.
66. **Yee SH, Lee K, Jerabek PA, Fox PT.** Quantitative measurement of oxygen metabolic rate in the rat brain using microPET imaging of briefly inhaled  $^{15}\text{O}$ -labelled oxygen gas. *Nucl Med Commun* 27: 573–581, 2006.
67. **Yoshizu A, Izumi Y, Park S, Sakai H, Takeoka S, Horinouchi H, Ikeda E, Tsuchida E, Kobayashi K.** Hemorrhagic shock resuscitation with an artificial oxygen carrier, hemoglobin vesicle, maintains intestinal perfusion and suppresses the increase in plasma tumor necrosis factor-alpha. *ASAIO J* 50: 458–463, 2004.
68. **Zauner A, Daugherty WP, Bullock MR, Warner DS.** Brain oxygenation and energy metabolism: part I-biological function and pathophysiology. *Neurosurgery* 51: 289–301; discussion 302, 2002.

